

Spectroscopy investigations reveal unprecedented details in the corrosion of AISI 1012 UPN profiles installed in a modernist building of beginning of 20th century

**José I. Iribarren^a, Francisco Liesa^b, Álvaro Meneguzzi^c, Carlos
Alemán^{a,d}, Elaine Armelin^{a,d,*}**

*^a Departament d'Enginyeria Química, EEBE, Universitat Politècnica de Catalunya, C/
d'Eduard Maristany, 10-14, Edifici I, E-08019, Barcelona, Spain.*

*^b Departament d'Enginyeria Mecànica, ETSEIB, Universitat Politècnica de Catalunya,
Av. Diagonal 647, E-08028, Barcelona, Spain.*

*^c Departamento de Engenharia de Minas, Metalúrgica e Materiais, Escola de
Engenharia, Universidade Federal do Rio Grande do Sul (UFRGS), Av. Bento Gonçalves,
9500 – 91501-970, Porto Alegre, RS, Brazil.*

*^d Barcelona Research Center in Multiscale Science and Engineering, Universitat Politècnica
de Catalunya, Campus Diagonal Besòs (EEBE), C/ d'Eduard Maristany 10-14, Edifici IS,
08019, Barcelona, Spain.*

Corresponding author: elaine.armelin@upc.edu

Abstract

In the present work, the corrosion affectation of an artistic and historical building, declared UNESCO World Heritage Site and constructed with AISI 1012 UPN profiles, was investigated. Micro-Raman and microscopy approaches highlight the complementarity and versatility of these techniques to evaluate the macroscopic and microscopic effect of the corrosion products in such reinforcing structures. The rust phases have been assessed by separating the oxide layers according to their environment placement and contaminants contact. The composition of iron oxides and oxyhydroxides in the metal surface depend not only on the oxygen concentration, but also on other elements that penetrated into the porous layers, as for example, chlorine ions, sulfur ions, and microorganisms. Taking into account the scarce information on the indoor corrosion of AISI 1012 steel, results obtained in this work are expected to help for understanding the long-term impact of such oxides and oxyhydroxides on the material durability, as well as on its structural maintenances.

Keywords: AISI 1012, micro-Raman; indoor corrosion, oxides, oxyhydroxides.

1. RESEARCH AIMS

The refurbishment of the Modernist complex named *Hospital de la Santa Creu i Sant Pau* (popularly known as *Hospital Sant Pau*) marks the start of a new era for the architectural buildings designed by Lluís Domènech i Montaner. The complex of the *Hospital Sant Pau*, which occupies a privileged location in the heart of the city of Barcelona, is one of the best examples of Catalan Modernism owing to its size, its structural characteristics and the artistic details of its buildings. The complex has 21 pavilions, being *Sant Manuel* building (Figure 1) one of the biggest inside the complex. During the restoration of *Sant Manuel* pavilion, serious problems of corrosion were detected on the UPN steel profiles placed as pillars, beams and reinforcing struts dome. In this study, thirteen fragments were extracted and evaluated using spectroscopy and microscopy tools. Considering the scarce corrosion studies about carbon steel AISI 1012, used as reinforcing material in such centenary edification, the present study reports for the first time the impact of oxides and oxyhydroxides growth on the deterioration of the whole complex during this large period.

2. INTRODUCTION

Iron oxides and hydroxides formed after the exposition of the metal to the environment constitute an old and mature investigation field. Fortunately, advances in technology, like micro-Raman (μ Raman) spectroscopy and powerful scanning electron microscopes, allow to investigate and assess new inputs about the influence of parameters related to humidity and ageing effects. Predict the steel-work construction life-time is a very difficult task, even though structural steel deterioration has been extensively studied considering different environments [1–5]. Many years ago, Neff *et. al* [6,7] reported the corrosion mechanism of ancient artefacts located on several cathedrals in France and around Europe [7] and exposed to the indoor atmosphere [6] by using micro-diffraction (μ XRD) and μ Raman spectroscopy. Those authors concluded that the main oxyhydroxide phase formed was goethite (α -FeOOH), whereas

lepidocrocite (γ -FeOOH) and akaganeite (β -FeOOH) occurred locally in the corroded products and were often correlated with cracks and pitting.

In general, the formation of rust products usually become increasingly severe in outside atmospheric conditions [8]. Nevertheless, scarce studies involving indoor affectation have been reported for mild carbon steel installed at beginning of 20th century.

Inspections using spectroscopy and microscopy techniques are the most useful procedures for fast detection of rust layers [9,10] since the development of new accessories, such as fiber portable optic probes, immersion probes, and special tips for working distance analysis, allows *in situ* analyses (*i.e.* non-contact and non-destructive analyses). Thus, the goal of the present work is to provide a broad spectroscopy and microscopy study about the corrosion effects of AISI 1012 installed for a very long period and exposed to humidity environment and concrete contact. The AISI 1012 (American Iron and Steel Institute) is a kind of mild and economic steel that, due to its chemical composition, exhibits better performance in its mechanical, weldability and machinability properties than other steels of the same group (AISI 1005, 1015, 1019, 1020) [11]. AISI 1012 steel can be cemented when a very hard surface with a tenacious center is required. Among its extensive applications, the most important are found in the manufacture of screws and other accessories, as well as in components for the automotive and railway sector.[12]

Although the diversity of iron composition in the physical chemistry field is extremely broad, one of the advantages of this discipline is the extensive and available information reported in the literature. In this work we applied the extensive knowledge on iron oxidation, previously reported, to the investigation of the deterioration of AISI 1012 reinforcing structures installed in a centenary building. The major strength of this work lies in the detailed understanding of how ions migrated from the outer to inner interface, and how this migration affected the growth of iron oxyhydroxides and oxides, after long-term of exposition. For this purpose, the correlation between the type of rust with the aggressiveness of the indoor

environment was achieved after a careful FTIR, μ Raman spectroscopies and SEM-EDX analyses. After this, results were compared with previously reported studies conducted with other grades of carbon steel.[13–16]

3. MATERIALS AND METHODS

3.1. Historical building and samples extraction

The *Sant Manuel* pavilion (Figure 1), located within Sant Pau's Modernist Hospital in Barcelona (Catalonia, Spain), with a total area of 2.563 m², was the object of this work. This building was projected by the architects *Lluís Domènech i Montaner* and *Pere Domènech i Roura* among years 1922 and 1925 and refurbished by architects *Víctor Argentí*, *Albert Casals* and *José Luis González* during three years (2009-2011). For the construction progresses, UPN profiles of steel (UPN100, UPN200 and UPN300), placed as pillars, beams and reinforcing struts dome, were employed as reinforcing metallic structures. As the profiles were not visible, with the obvious exception of structures with extreme corrosion and cement deterioration, the engineers working in the restoration had to prepare the walls for samples extraction, making then accessible by removing the cement and stones. A random selection of the different zones into the metallic skeleton was chosen to obtain a representative overview of the metallic structure, getting comparative results about the global situation of the building deterioration. Samples were selected in accessible points, minimizing the structural affectation of the building (Figure 2). The size of the pieces extracted was about 5 × 5 cm² with variable thicknesses, which ranged from 0.5 to 1.0 cm. The total of samples analyzed varied from twenty to twenty-four depending on the size and purpose of analysis. Table S1 displays the first thirteen samples.

After accurate extraction of samples, gravimetric, spectroscopic and microscopic studies were performed to catalogue the corrosion state of *Sant Manuel* pavilion structure according to its degree of affectation [17–19].

3.2. Materials

The metallic structures of *Sant Manuel* pavilion were built using European Standard Channels-UPN profiles of carbon steel AISI/SAE 1012 (American Iron and Steel Institute and the Society of Automotive Engineers classification). The two types of UPN profiles studied are UPN100 and UPN200. Additional information about their geometry was described elsewhere [20]. The chemical composition was confirmed by the standard ASTM E350-12 [21] and is reported in the electronic supplementary information (ESI). The study has been focused in AISI 1012 profiles in direct contact with cement, close to installed water pipes, as well as in structures without surrounding pipelines (Figure 2).

3.3. Physical-chemistry characterization of iron oxides and oxyhydroxides

The chemical composition of the several layers of iron products was determined by infrared and μ Raman spectroscopies. For FTIR studies a Nicolet 6700 FTIR spectrometer equipped with transmission accessory and Omnic software was employed. The spectra were collected in the range of 400-4000 cm^{-1} with a resolution of 8 cm^{-1} (total of 120 scans). Disks composed by KBr and oxide were prepared using 3% w/w of oxide powder, previously extracted from the corroded steel and mortared in a mortar until homogenous particle fineness, and pressed with hydraulic pressure equipment (8 tons). Raman spectra were recorded with Horiba Jobin Yvon equipment (model Abran HR800) using a source of 532 nm and a diffraction grating of 600 nm. An Olympus BX-51 light polarizing microscope, operating in reflection mode with an Olympus C3030Z digital camera coupled, was used to observe the pitting attack. Previously, the specimen cross-sections were carefully polished to mirror with Bhuelher 2 Speed Gainer-Polisher.

Field-emission scanning electron microscopy (FE-SEM) and energy dispersive X-ray (EDX) of iron oxides were employed to observe the morphology and to obtain the semi-quantitative composition, respectively. This study was carried out using a Focused Ion Beam Zeiss Neon 40 scanning electron microscope equipped with EDX spectroscopy system and operating at 5 kV and 30 kV, respectively. In this case, flakes of iron oxides were detached *in*

situ from the specimen surface and both the external side (oxygen-rich) and internal side (metal-rich) were examined. For a detailed experimental setup refers to the section 3.3 in the ESI. The corrosion rate (mm/year) of UPN profiles was estimated by gravimetric analysis (ESI).

Six samples among thirteen selected specimens, which are classified in Table S1, were considered as the most representative samples of the different rust phases achieved in Sant Manuel pavilion. Table 1 shows the photographs of the corroded AISI 1012 samples, with a qualitative correlation between the degree of corrosion attack and the placement of samples.

4. RESULTS AND DISCUSSION

4.1. Infrared and μ Raman spectroscopy analyses

The application of spectroscopic methods, such as Raman, infrared and Mössbauer spectroscopies, has been highlighted to be complementary techniques for the identification of oxides in mild iron [22–25]. The major IR absorption bands in both non-adherent rust products encountered in AISI 1012 steel (*i.e.* considering the internal side of the rust flakes) and external layers of samples with mild corrosion attack are 542 cm^{-1} and 464 cm^{-1} (Figure S1a), which is consistent with hematite ($\alpha\text{-Fe}_2\text{O}_3$) composition. Some less intense peaks corresponding to goethite are also present. However, if the corrosion products were located in the outer layer, it represents a mixture of non-adherent oxides and oxyhydroxides (Figure S1b) with absorption bands characteristic of goethite (W-shaped signal at 795 and 891 cm^{-1}), lepidocrocite (sharp and broad bands at 1024 and $\sim 3121\text{ cm}^{-1}$), magnetite (below 700 cm^{-1}) and akaganéite (broad bands at ~ 420 , 1632 , 1483 and 3430 cm^{-1})[22–25].

Additionally, among the ferric oxyhydroxides, $\beta\text{-FeOOH}$ is considered to be the most detrimental to the corrosion resistance of steel because the chemical structure of akaganéite contains chlorine ions (Cl^-) [26]. This type of ion is associated to a pitting phenomenon on metallic substrates. The presence of absorption peaks in the infrared spectra of akaganéite

structures is a clear evidence of the fast metal deterioration, when installed close to water pipes, *i.e.* with high humidity or when covered by Portland cement.

Raman spectra confirmed the oxides and hydrated oxyhydroxides mentioned before. Lepidocrocite (γ -FeOOH), which is usually formed in the early stages of atmospheric corrosion (Table 1, sample M10) only. This transforms into goethite (α -FeOOH) (Table 1, samples M1 and M3) with increasing exposure time, which is in accordance with the recent observations of Yucel *et. al* [10]. The main phases observed for specimens with severe (M1) and advanced corrosion degrees (M3) are lepidocrocite (γ -FeOOH) and goethite (α -FeOOH), as can be seen in Figures 3a-b. The intensity of the peaks changed due to the heterogeneous concentration of these corrosion products in the outer layer, as is shown by the broad absorption bands obtained for the specimen M1. In opposition, in sample M3, the major contribution comes from goethite with strong peaks at 390 cm^{-1} and 679 cm^{-1} , respectively [27].

Furthermore, the Raman spectrum of the M10 sample (Figure 3c), with moderate corrosion degree, shows pure γ -FeOOH phase. This identification is evidenced by the characteristic features at 249 and 377 cm^{-1} and corroborated by four additional peaks at 216 , 300 , 523 and 654 cm^{-1} [28]. Again, akaganéite molecules (β -FeOOH) were identified in a panel specifically extracted from a UPN profile close to water pipes (MCB), showing very intense absorption bands at 307 , 385 and 720 cm^{-1} (Figure 3d).

Comparison of the samples with scarce delamination, like specimen M4 in Figure 3e, with other having similar rust products, like MSB in Figure 3f, which are both far from gutter pipes or pipelines, indicates that the major iron oxide structures correspond to magnetite (Fe_3O_4 ; 660 cm^{-1}) [29] and hematite (α - Fe_2O_3 ; 224 , 290 , 410 , 500 , 610 cm^{-1}) [3]. These data confirm the mechanism reported by several authors [10,30–32] with respect to the products identified in the oxide layer of weathering steel exposed to various atmospheres. Furthermore, magnetite (Fe_3O_4) and hematite (α - Fe_2O_3) were not detected on the surface of specimens classified with

severe and advanced corrosion, corroborating our hypothesis about the growing of rust layers (section 4.3 and ESI).

4.2. Mapping of the evolution of oxides and oxyhydroxides formation in AISI 1012 surface. Correlation with the environment aggressiveness

A detailed inspection of localized pitting corrosion in a sample with advanced corrosion degree (MCB, Table 1) allowed the detection of oxide layers with chlorine and calcium ions within the evaluated region (Figure 4). SEM micrograph showed in the Figure 4a represents one of the several localized corrosion attacks found in the AISI 1012 surface (polished cross-sectional cut). EDX analyses allowed us to corroborate that the centenary steel is free of metals like chromium and copper, which would accelerate the corrosion mechanism. The semi-quantitative EDX concentration was found to be (in atomic %): Fe > 99%, C ~ 0.80% and Mn 0.37-0.40%. The EDX from the metal surface (cross-section of the inner metal interface) has a high concentration of Mn, as shown in the Figure 4b, whereas the EDX of the main rust products inside the pitting zone (Figure 4c) revealed Fe, O and C as principal elements. In addition to the oxides and hydrated oxyhydroxides discussed before, the presence of chlorine salts was observed as spherical particles trapped inside the iron oxide molecules (Figure 4d), as well as the presence of calcium. The presence of calcium carbonate, calcium silicate hydrate, and calcium chloride substances within the cement, that is in direct contact with the metallic structures, are responsible for the AISI 1012 depassivation and pitting corrosion, as stated in our previous electrochemical study [20]. In such previous work the presence of calcium chloride (CaCl₂) salt was proved by FTIR and XRD analyses.[20] EDX results (Figure 4d) led us to confirm, once again, that chlorine contamination came from the Portland cement, which was in direct contact with the sample MCB for several years, migrating to the iron oxide layer after hydration. Mechanism of depassivation of steel reinforcement and, consequently, steel pitting corrosion under contact with cement, was reported by Bertolini & Redaelli.[33]

Furthermore, results derived from the Raman analyses of the cross-section made on another zone of sample MCB (Figures 4e-f) confirmed the above mentioned observations. From the outer layer (oxygen-rich) to the inner (metal-oxide interface) (Figure 4g):

(i) The external oxide is composed, mainly, by goethite phase (curves 1 and 2), as is demonstrated by the intense absorption band at 385 cm^{-1} , attributed to Fe-O-Fe and -OH symmetric stretching; 298 cm^{-1} from Fe-O symmetric bending; 550 cm^{-1} from Fe-OH asymmetric stretching; and 676 cm^{-1} from Fe-O symmetric stretching. No evidence of akaganéite or lepidocrocite was found in this zone (absorption bands described in section 4.1).

(ii) The curve 3, which corresponds to the intermediate layer, has broader peaks than the outer layer, and reveals the co-existence of two phases, supposedly goethite and magnetite, if we compare to the spectrum of the metal-oxide interface (curve 4). No evidence of hematite or lepidocrocite were detected in this zone (absorption bands described in section 4.1).

(iii) The Raman spectrum shows a broad absorption band at 666 cm^{-1} , which can be attributed to Fe-O symmetric stretching of magnetite structures. This fact is in accordance with our SEM observations (section 4.3 and ESI) and is in agreement with previous works with other mild steel composition [6,27,32].

The mechanism for AISI 1012 steel profiles occurs in different stages and can be summarized as follow. The first step is the obtaining of a very adherent wüstite (FeO) composition that rapidly converts into magnetite (Fe₃O₄) (Figure S15). Therefore, aggressive iron oxides (second step), which corresponds to compositions with detrimental effects for the steel installation (magnetite, hematite, goethite, and akaganéite), are detected in the external layers. These show high oxygen concentration. In such cases, the rust layers can be easily detached (Table 1, samples M3, M10 and MCB) and their chemical composition was found to be strictly related to goethite, akaganéite and lepidocrocite phases. The composition of iron oxides in UPN profiles depends not only on the oxygen concentration but also on other elements that penetrated into the oxide layers, as for example, chlorine and sulfur ions, and

microorganisms. The harshest chemical agent found is chlorine ions (Cl^-). Lately, Li and co-workers [34] have established the mechanism of formation of akaganeite inside the structure of rust layer obtained after several dry-wet cycles of corrosion test. They proved, by XRD, SEM and electron probe microanalysis (EPMA) that chlorine elements aggregate between rust layers and the substrate, and were active and participated in the formation of akaganeite, even after the removing of rust layer.

4.3. Microscopy study and corrosion mechanism

SEM micrographs revealed several cracking zones, flaking and high porosity topographies when evaluating the oxides layers on AISI 1012 steel. The distribution of corrosion products in the outer layers is irregular and consists of different crystalline phases. In samples with high oxide delamination, like M1, M3 and MCB (Table 1), the flakes were detached from the specimen surface and both the external side (oxygen-rich) and internal side (less oxygen-rich) were observed. In the outer layers a mixture of well-known morphologies typically found for akaganéite (Figure 5), goethite (Figure S3) and lepidocrocite (Figure S4) were found. Akaganéite ($\beta\text{-FeOOH}$) appeared meanly on specimens close to gutter pipes and covered by cement, as stated before for samples M3 and MCB, and has an elongated crystalline appearance, sometimes aggregated as distorted cubes (Figure 5b). Figures 5c-d show SEM micrographs of areas exhibiting abundant elongated crystals of akaganéite. The other sequential morphologies found and their respective classification were included in the ESI, as well as a detailed discussion. Unfortunately, in this study we did not have enough evidences to corroborate the presence of maghemite structures ($\gamma\text{-Fe}_2\text{O}_3$) and further EDX characterizations would be necessary for the quantification of Fe:O atomic concentration ratio.

There is a broad consensus in the scientific community about the complex and inhomogeneous composition of the rust film formed onto carbon steel surfaces under indoor atmosphere. In fact, several researchers have concluded that such rust growth consists of mainly two layers [3,27,28,30,35]: (i) a regular inner layer with a spinel structure that adheres very

well to the metal surface, which is composed of magnetite and maghemite and Fe(II)/Fe(III) oxides; (ii) a second layer that is more loosely composed of hydrated iron oxides (like $\text{Fe}_2\text{O}_3 \cdot \text{H}_2\text{O}$) and oxyhydroxides, like that described in the present work. Additionally, in a very recent study, Chew *et al.*[36] used density functional theory (DFT) calculations to demonstrate step by step how the electrochemical processes of iron oxidation and oxygen reduction reactions occurs in neutral and alkaline conditions. In summary, they corroborated with a theoretical model the experimental mechanisms usually found by experimental researchers. Other relevant works related with these processes are those developed by Stratmann *et al.* [37] and De la Fuente and co-workers.[38]

Attaining the best life-cycle performance of a structural reinforcing UPN profile, especially that made of unpainted carbon steel, the preliminary detection and control of corrosion phenomena is of utmost importance. For this reason, one of the possibilities to monitor the corrosion impact on such old and refurbished buildings would be leave some sections of pillar accessible. They will facilitate the conduction of fast spectroscopic analyses (*e.g.* by using portable Raman systems and/or fiber optic probes) and also for the installation of humidity control sensors close or in contact with the UPN profiles, inside such pillar sections. The maintenance and rust-monitoring is desirable to be carried out every 10 years after installation, particularly if it is not covered by cement; or even every 5 years if the metal surface is in contact with other materials or installed in high humidity indoor conditions.

5. CONCLUSIONS

Given the architectural importance of the *Sant Manuel* historical building, the accurate determination of the oxide and oxyhydroxides layers performed in this work were of fundamental relevance for its refurbishment. Comparisons of both spectroscopy and microscopy results, combined with the macroscopic observations of the weathering effect on thirteen samples extracted from AISI 1012 structural reinforcing steel, helped to design a

mechanism for the different rust layer depositions on the metal surface. To conclude, the metal-oxide interface was characterized by the growth of a passive film on iron surface, which slowly converted into oxygen-rich iron oxides after a long period of time, in the indoor environment.

Particularly, infrared and μ Raman spectroscopies, as well as scanning electron microscopy revealed the presence of hematite (α -Fe₂O₃), goethite (α -FeOOH), lepidocrocite (γ -FeOOH); magnetite (Fe₃O₄), and in some cases, akaganéite (β -FeOOH) for the non-adherent rust flakes. Akaganéite was mainly found on samples installed close to gutter pipes and covered by cement, *i.e.* under direct contact with contaminant moisture. When non-adherent layers appear onto metal surface, their elimination is of utmost importance.

In this work, we used spectroscopy and microscopy techniques and the well-known mechanism of rust formation extensively reported by other authors to detect the most harmful oxide layers in the ancient carbon steel structure of *Sant Manuel* pavilion.

In summary, our study is consistent with the model of rust growing in which the oxides evolution is being formed after some phase transformations and after very long process of indoor exposition to humidity and contaminants.

At present, the *Sant Manuel* pavilion is completely restored, the problems of corrosion were solved and the refurbishment was finished in 2012. Currently, this building is used as headquarters of the United Nations University Institute on Globalization, Culture and Mobility and *Casa Àsia*.

Acknowledgements

This work has been supported by MICINN and FEDER funds (RTI2018-098951-B-I00) and Agència de Gestió d'Ajuts Universitaris i de Recerca (2017SGR359). C. Alemán acknowledges the award “ICREA Academia 2015” for excellence in research funded by the Generalitat de Catalunya (Catalonia-Spain). We are also grateful to Dr. F. Heredero and to Dr. T. Trifonov for their help with the microstructure and SEM analyses, respectively.

References

- [1] P. Albrecht, T.T. Hall, Atmospheric Corrosion Resistance of Structural Steels, *J. Mater. Civ. Eng.* 15 (2003) 2–24. doi:10.1061/(ASCE)0899-1561(2003)15:1(2).
- [2] T. Murata, Weathering Steel, *Uhlig's Corros. Handb.* (2011) 621–631. doi:10.1002/9780470872864.ch48.
- [3] D. de la Fuente, I. Díaz, J. Simancas, B. Chico, M. Morcillo, Long-term atmospheric corrosion of mild steel, *Corros. Sci.* 53 (2011) 604–617. doi:10.1016/j.corsci.2010.10.007.
- [4] M. Morcillo, B. Chico, I. Díaz, H. Cano, D. de la Fuente, Atmospheric corrosion data of weathering steels. A review, *Corros. Sci.* 77 (2013) 6–24. doi:10.1016/j.corsci.2013.08.021.
- [5] M. Morcillo, I. Díaz, B. Chico, H. Cano, D. de la Fuente, Weathering steels: From empirical development to scientific design. A review, *Corros. Sci.* 83 (2014) 6–31. doi:10.1016/j.corsci.2014.03.006.
- [6] D. Neff, S. Reguer, L. Bellot-Gurlet, P. Dillmann, R. Bertholon, Structural characterization of corrosion products on archaeological iron: an integrated analytical approach to establish corrosion forms, *J. Raman Spectrosc.* 35 (2004) 739–745. doi:10.1002/jrs.1130.
- [7] D. Neff, L. Bellot-Gurlet, P. Dillmann, S. Reguer, L. Legrand, Raman imaging of ancient rust scales on archaeological iron artefacts for long-term atmospheric corrosion mechanisms study, *J. Raman Spectrosc.* 37 (2006) 1228–1237. doi:10.1002/jrs.1581.
- [8] J. Alcántara, B. Chico, J. Simancas, I. Díaz, D. de la Fuente, M. Morcillo, An attempt to classify the morphologies presented by different rust phases formed during the exposure of carbon steel to marine atmospheres, *Mater. Charact.* 118 (2016) 65–78. doi:10.1016/j.matchar.2016.04.027.
- [9] M.K. Nieuwoudt, J.D. Comins, I. Cukrowski, The growth of the passive film on iron in

- 0.05 M NaOH studied in situ by Raman microspectroscopy and electrochemical polarization. Part II: In situ Raman spectra of the passive film surface during growth by electrochemical polarization, *J. Raman Spectrosc.* 42 (2011) 1353–1365.
doi:10.1002/jrs.2842.
- [10] N. Yucel, A. Kalkanli, E.N. Caner-Saltik, Investigation of atmospheric corrosion layers on historic iron nails by micro-Raman spectroscopy, *J. Raman Spectrosc.* 47 (2016) 1486–1493. doi:10.1002/jrs.5014.
- [11] J.E. Bringas, Handbook of comparative world steel standards. ASTM DS67B, ASTM International, 2004.
- [12] V. Agarwal, Steel Handbook : A Guide to World Equivalent Steel Grades, Vishwas Agarwal, Techno-Publications, Mumbai, India, 2012.
- [13] G. Croci, General methodology for the structural restoration of historic buildings: The cases of the Tower of Pisa and the Basilica of Assisi, *J. Cult. Herit.* 1 (2000) 7–18.
doi:10.1016/S1296-2074(99)00119-3.
- [14] M. Mosoarca, V. Gioncu, Structural safety of historical buildings made of reinforced concrete, from Banat region--Romania, *J. Cult. Herit.* 14 (2013) e29–e34.
- [15] P.S. Wu, C.M. Hsieh, M.F. Hsu, Using heritage risk maps as an approach to estimating the threat to materials of traditional buildings in Tainan (Taiwan), *J. Cult. Herit.* 15 (2014) 441–447. doi:10.1016/j.culher.2013.10.005.
- [16] F. Karaca, Mapping the corrosion impact of air pollution on the historical peninsula of Istanbul, *J. Cult. Herit.* 14 (2013) 129–137. doi:10.1016/j.culher.2012.04.011.
- [17] H. de la S.C. i S.P. Fundació Privada, Restoration Sant Manuel Pavillion, 2012. (n.d).
<http://www.santpaubarcelona.org/dev/en/pavello-de-sant-manuel>.
- [18] E. European Regional Development Fund, Rehabilitación y consolidación del pabellón Sant Manuel como sede del Instituto UNU-IIAOC, 2007.
- [19] Convention concerning the protection of the world cultural and natural heritage.,

Naples, Italy, 1997.



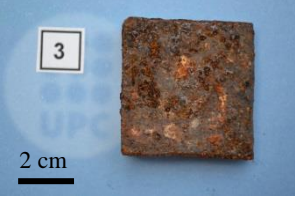



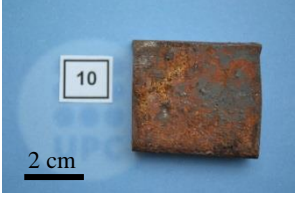
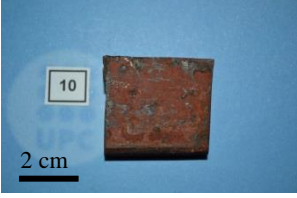
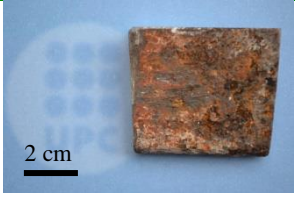
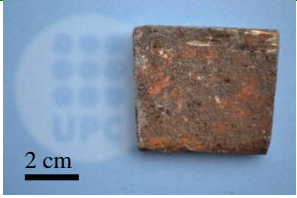


- [20] J.I. Iribarren, F. Liesa, C. Alemán, E. Armelin, Corrosion rate evaluation by gravimetric and electrochemical techniques applied to the metallic reinforcing structures of a historic building, *J. Cult. Herit.* 27 (2017) 153–163. doi:10.1016/j.culher.2017.04.009.
- [21] ASTM E350 - 18 Standard Test Methods for Chemical Analysis of Carbon Steel, Low-Alloy Steel, Silicon Electrical Steel, Ingot Iron, and Wrought Iron, 2018.
- [22] R. Balasubramaniam, A.V.R. Kumar, P. Dillmann, Characterisation of rust on ancient Indian iron, *Curr. Sci.* 85 (2003) 1546–1555.
- [23] T.D. Glotch, M.D. Kraft, Thermal transformations of akaganéite and lepidocrocite to hematite: Assessment of possible precursors to Martian crystalline hematite, *Phys. Chem. Miner.* 35 (2008) 569–581. doi:10.1007/s00269-008-0249-z.
- [24] R. V Morris, H. V Lauer, C.A. Lawson, E.K. Gibson, G.A. Nace, C. Stewart, Spectral and other physicochemical properties of submicron powders of hematite (α -Fe₂O₃), maghemite (γ -Fe₂O₃), magnetite (Fe₃O₄), goethite (α -FeOOH), and lepidocrocite (γ -FeOOH), *J. Geophys. Res.* 90 (1985) 3126–44.
- [25] M. Ma, Y. Zhang, W. Yu, H. Shen, H. Zhang, N. Gu, Preparation and characterization of magnetite nanoparticles coated by amino silane, *Colloids Surfaces A Physicochem. Eng. Asp.* 212 (2003) 219–226. doi:10.1016/S0927-7757(02)00305-9.
- [26] T. Nishimura, H. Katayama, K. Noda, T. Kodama, Electrochemical Behavior of Rust Formed on Carbon Steel in a Wet/Dry Environment Containing Chloride Ions, *CORROSION.* 56 (2000) 935–941. doi:10.5006/1.3280597.
- [27] M.A. Legodi, D. de Waal, The preparation of magnetite, goethite, hematite and maghemite of pigment quality from mill scale iron waste, *Dye. Pigment.* 74 (2007) 161–168. doi:10.1016/J.DYEPIG.2006.01.038.
- [28] S.J. Oh, D.C. Cook, H.E. Townsend, Characterization of Iron Oxides Commonly

- Formed as Corrosion Products on Steel, *Hyperfine Interact.* 112 (1998) 59–66.
doi:10.1023/A:1011076308501.
- [29] F. Pérez, C. Barrero, O. Amache, L. Sánchez, S. Peñaranda, K. García, M. Pérez, Caracterización De Herrumbres En Procesos De Corrosión De Aceros En Inmersión Total, *Rev. Colomb. Física.* 39 (2007) 83–86.
- [30] R.A. Antunes, I. Costa, D.L.A. De Faria, Characterization of corrosion products formed on steels in the first months of atmospheric exposure, *Mater. Res.* 6 (2003) 403–408. doi:10.1590/S1516-14392003000300015.
- [31] X. Nie, X. Li, C. Du, Y. Huang, H. Du, Characterization of corrosion products formed on the surface of carbon steel by Raman spectroscopy, *J. Raman Spectrosc.* 40 (2009) 76–79. doi:10.1002/jrs.2082.
- [32] J. Monnier, L. Bellot-Gurlet, D. Baron, D. Neff, I. Guillot, P. Dillmann, A methodology for Raman structural quantification imaging and its application to iron indoor atmospheric corrosion products, *J. Raman Spectrosc.* 42 (2011) 773–781. doi:10.1002/jrs.2765.
- [33] L. Bertolini, E. Redaelli, Depassivation of steel reinforcement in case of pitting corrosion: detection techniques for laboratory studies, *Mater. Corros.* 60 (2009) 608–616. doi:10.1002/maco.200905276.
- [34] H. Xiao, W. Ye, X. Song, Y. Ma, Y. Li, Formation process of akaganeite in the simulated wet-dry cycles atmospheric environment, *J. Mater. Sci. Technol.* 34 (2018) 1387–1396. doi:10.1016/j.jmst.2017.06.020.
- [35] R.A. Antunes, R.U. Ichikawa, L.G. Martinez, I. Costa, Characterization of corrosion products on carbon steel exposed to natural weathering and to accelerated corrosion tests, *Int. J. Corros.* 2014 (2014) ID 419570, 9 pages. doi:10.1155/2014/419570.
- [36] K.H. Chew, R. Kuwahara, K. Ohno, First-principles study on the atomistic corrosion processes of iron, *Phys. Chem. Chem. Phys.* 20 (2018) 1653–1663.

doi:10.1039/c7cp04022a.

- [37] M. Stratmann, K. Bohnenkamp, H.-J. Engell, An electrochemical study of phase-transitions in rust layers, *Corros. Sci.* 23 (1983) 969–985. doi:10.1016/0010-938X(83)90024-0.
- [38] M. Morcillo, J. Alcántara, I. Díaz, B. Chico, J. Simancas, D. De la Fuente, D. de la Fuente, Marine atmospheric corrosion of carbon steels, *Rev. Metal.* 51 (2015) e045. doi:10.3989/revmetalm.045.

Table 1. Classification of AISI 1012 UPN samples according to their qualitative degree of corrosion, observed macroscopically, and confirmed by spectroscopic techniques. Six samples from the thirteen selected specimens (Table S1) were considered to be the most representative of the different rust phases observed in the carbon steel.

<i>Sample</i>	<i>Degree of corrosion</i>	<i>Side A</i>	<i>Side B</i>
M1^{a)}	Severe, loss of geometry		
M3^{a)}	Advanced, abundant oxide delamination		
M4^{b)}	From moderate to advanced, scarce oxide delamination		
M10^{b)}	From moderate to advanced oxide delamination		
MCB^{a)}	Advanced, similar to M3 Abundant oxide delamination		
MSB^{b)}	Moderate, scarce oxide delamination		

Note: ^{a)} Nodes from UPN profiles close to gutter pipes (cgp) around, ^{b)} Nodes from UPN profiles without gutter pipes (wgp) around.

Captions to Figures

Figure 1. View of the *Hospital de la Santa Creu i Sant Pau* building plans showing the location of *Sant Manuel* pavilion. Adapted from the web page www.santpau.cat. Copyright of Private Foundation of Hospital de la Santa Creu i Sant Pau.

Figure 2. Corroded UPN profiles close to gutter pipes and pipelines: (a) sample M3, (b) sample M12, and (c) sample M1. Corroded UPN profiles without gutter pipes or pipelines around: (d) sample M6, (e) sample M11, and (f) sample MSB, node from reinforcing roof truss. Red marks indicate the zones where the samples for the analyses of rust layers were extracted. See Table S1 for codes identification.

Figure 3. Optical micrographs from rough oxide surfaces (left) and Raman absorption bands from the point highlighted (right) on the micrograph for: (a) M1; (b) M3; (c) M10; (d) MCB; and (e) MSB, extracted from AISI 1012 steel profiles installed in *Sant Manuel* pavilion. Scale bars inset: 50 μm .

Figure 4. (a) SEM micrograph of a typical corrosion layout observed on MCB sample (UPN profiles close to gutter pipes). EDX spectra obtained for each zone shown on (a), which correspond to: (b) carbon steel, (c) iron oxides and (d) spherical particles. (e-f) Low and high magnification optical micrographs from another cross-section of sample MCB analyzed with μRaman (g). The numbers inset are from outer to inner rust formation (1 to 4) showed in (f). Scale bars are indicated in all cases.

Figure 5. SEM micrographs corresponding to akaganéite crystalline phase found indistinctly in samples M1, M3 and MCB: (a) low magnification of rust outer layer, showing some flakes and cracks; (b) high magnification of image (a, inset), with aggregated particles (distorted cube geometry); (c) high magnification of elongated crystals; and (d) very high magnification of the previous micrograph showing an area rich in elongated crystals.

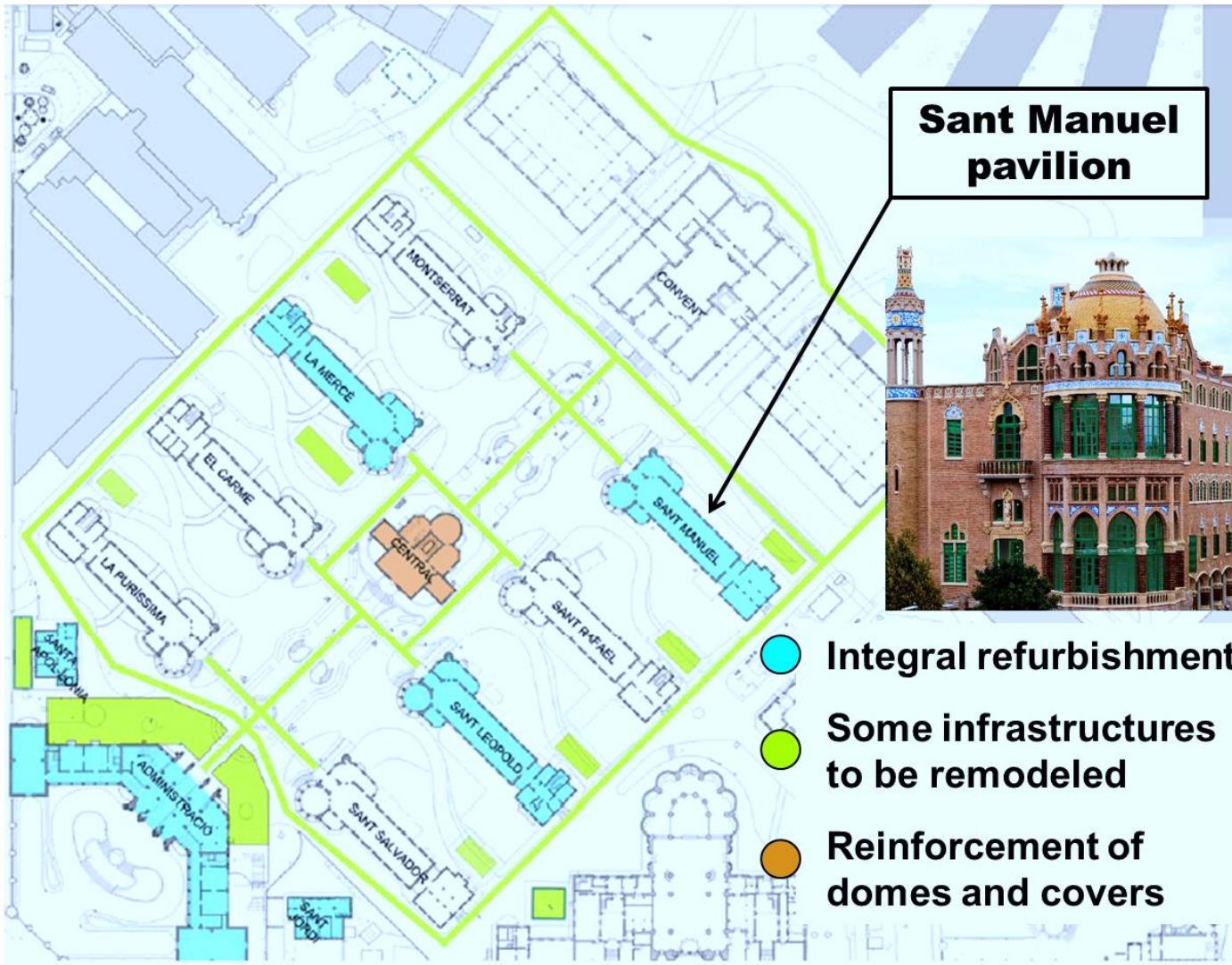


Figure 1

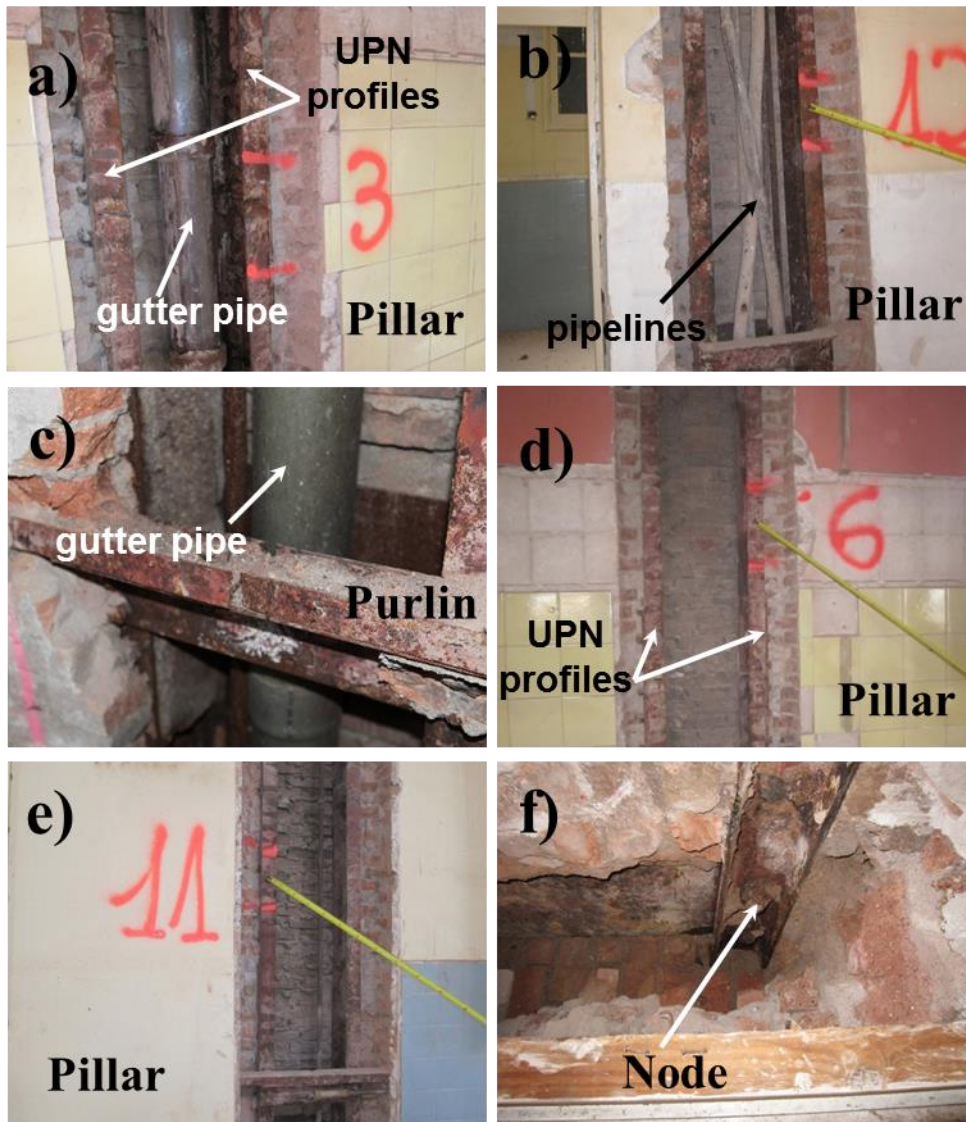


Figure 2

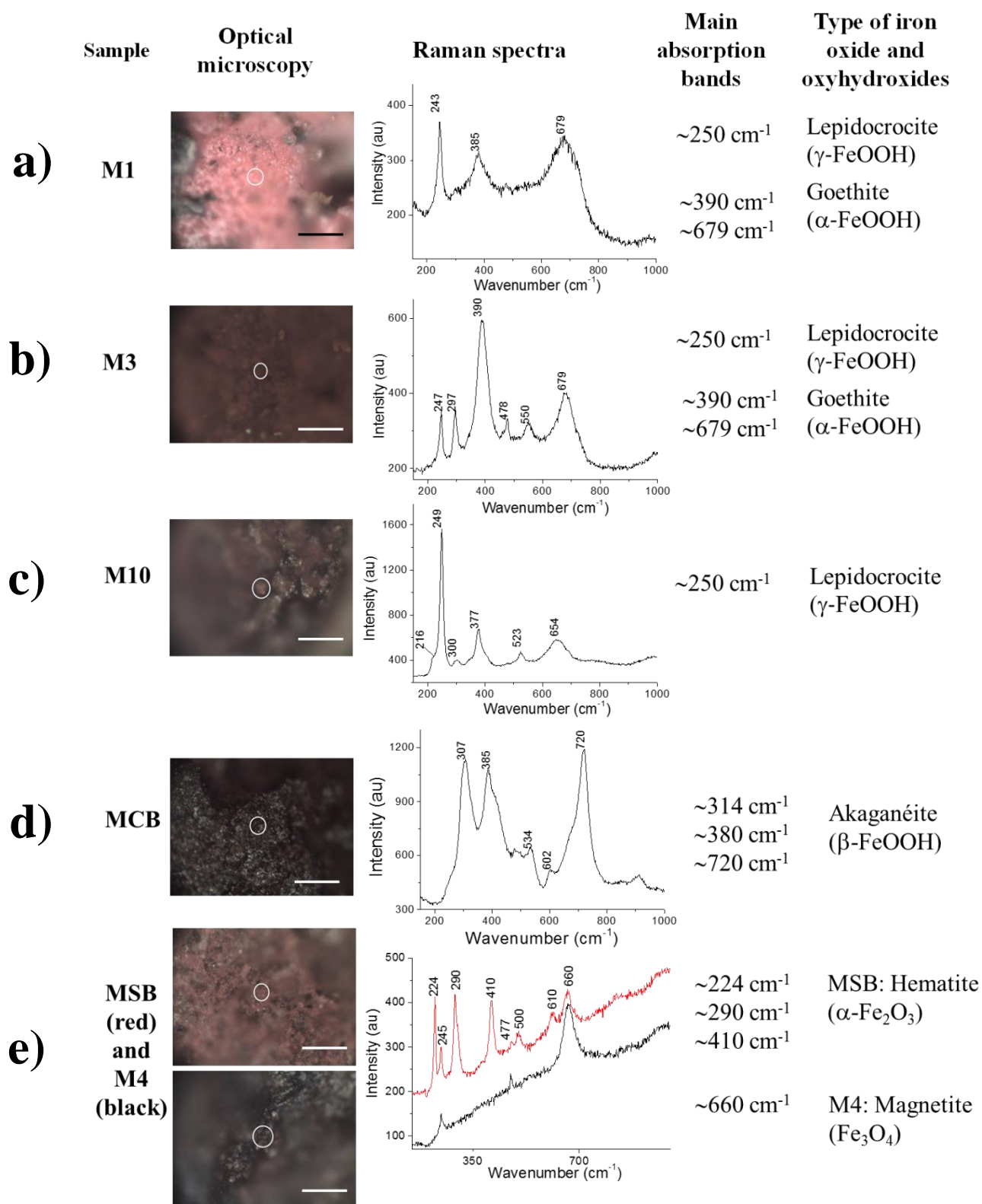


Figure 3

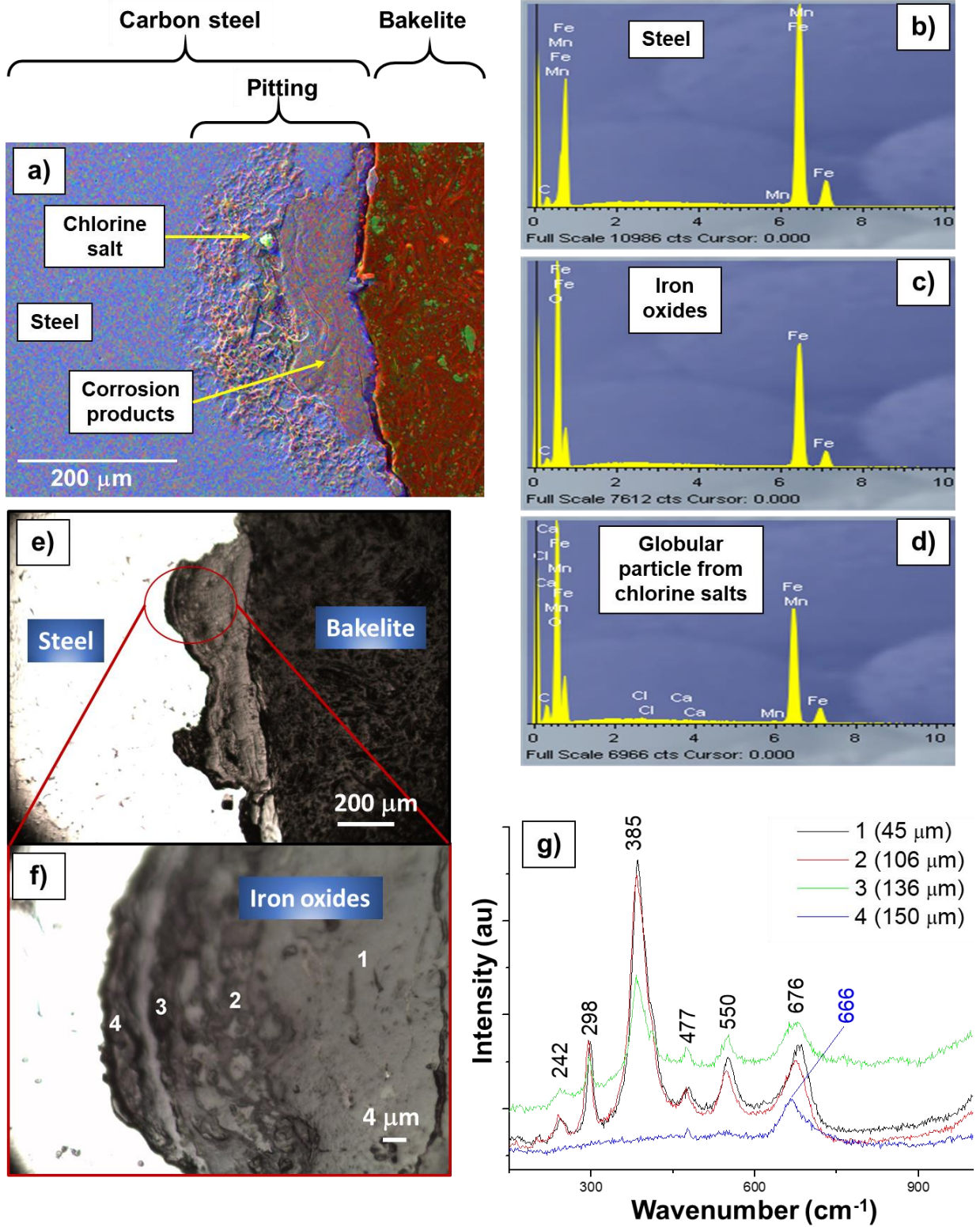


Figure 4

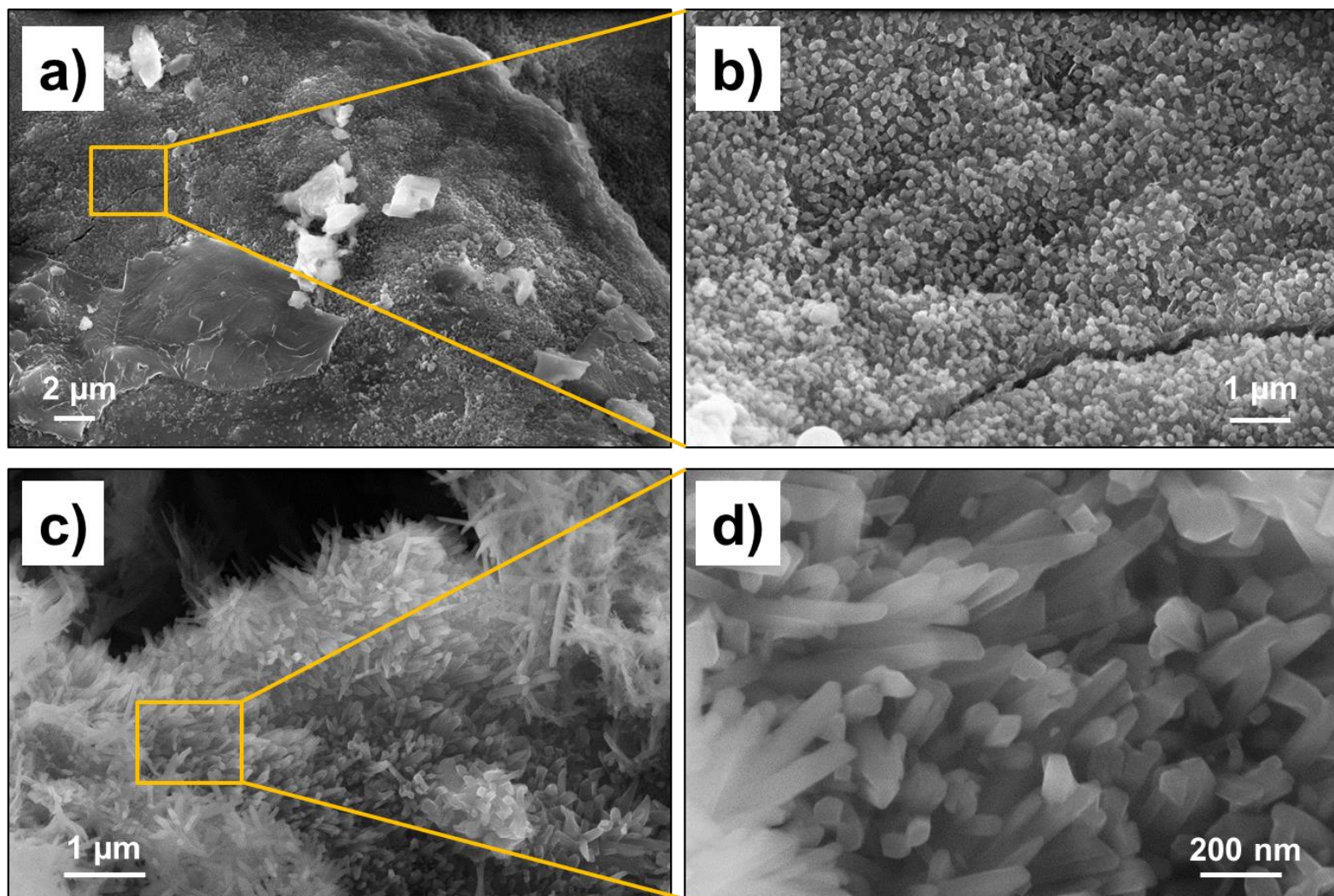


Figure 5